NMR structure of a lytic polysaccharide monooxygenase provides insight into copper binding, protein dynamics, and substrate interactions

Finn L. Aachmann[a,1], Morten Sørlie[b], Gudmund Skjåk-Bræk[a], Vincent G. H. Eijsink[b], and Gustav Vaaje-Kolstad[b,1]

[a]Department of Biotechnology, NOBIOPOL, Norwegian University of Science and Technology, NO-7491 Trondheim, Norway; and [b]Department of Chemistry, Biotechnology and Food Science, Norwegian University of Life Sciences, NO-1432 Aas, Norway

Edited by Arnold L. Demain, Drew University, Madison, NJ, and approved September 27, 2012 (received for review May 30, 2012)

Lytic polysaccharide monooxygenases currently classified as carbohydrate binding module family 33 (CBM33) and glycoside hydrolase family 61 (GH61) are likely to play important roles in future biorefining. However, the molecular basis of their unprecedented catalytic activity remains largely unknown. We have used NMR techniques and isothermal titration calorimetry to address structural and functional aspects of CBP21, a chitin-active CBM33. NMR structural and relaxation studies showed that CBP21 is a compact and rigid molecule, and the only exception is the catalytic metal binding site. NMR data further showed that His28 and His114 in the catalytic center bind a variety of divalent metal ions with a clear preference for Cu^{2+} (K_d = 55 nM; from isothermal titration calorimetry) and higher preference for Cu^{1+} (K_d ~ 1 nM; from the experimentally determined redox potential for CBP21-Cu^{2+} of 275 mV using a thermodynamic cycle). Strong binding of Cu^{1+} was also reflected in a reduction in the pK_a values of the histidines by 3.6 and 2.2 pH units, respectively. Cyanide, a mimic of molecular oxygen, was found to bind to the metal ion only. These data support a model where copper is reduced on the enzyme by an externally provided electron and followed by oxygen binding and activation by internal electron transfer. Interactions of CBP21 with a crystalline substrate were mapped in a $^2H/^1H$ exchange experiment, which showed that substrate binding involves an extended planar binding surface, including the metal binding site. Such a planar catalytic surface seems well-suited to interact with crystalline substrates.

cellulose | biomass

Chitin and cellulose represent some of nature's largest reservoirs of organic carbon in the form of monomeric hexose sugars (*N*-acetyl-glucosamine and glucose, respectively) linearly linked by β-1,4 glycosidic bonds. In their natural form, both polysaccharides are organized in crystalline arrangements that make up robust biological structures, like crustacean cuticles (chitin) or plant cell walls (cellulose). Although this crystalline nature is crucial for biological function, it provides a thorough challenge in industrial biorefining of biomass, where efficient enzymatic depolymerization of particularly cellulose is a critical step.

Enzymatic degradation of recalcitrant polysaccharides has traditionally been thought to occur through the synergistic action of hydrolytic enzymes that have complementary activities (1, 2). Endo-acting hydrolases make random scissions on the polysaccharide chains, whereas exo-acting processive hydrolases mainly target chain ends. However, during the last 2 years, a new enzyme family targeting recalcitrant polysaccharides has been identified, namely the lytic polysaccharide monooxygenases [LPMOs; also referred to as lytic polysaccharide oxidases (3), polysaccharide monooxygenases (4), and oxidohydrolases (5)]. In contrast to the classic hydrolytic enzymes that comprise many enzyme families, LPMOs only group into two distinct families (6): carbohydrate binding module family 33 (CBM33), with bacterial, viral, and some eukaryotic members, and glycoside hydrolase family 61 (GH61), with so far, only fungal members. The two LPMO families share a common fold, with a flat substrate binding surface that contains a metal binding site that includes two conserved histidines (5, 7, 8) (see below).

LPMO activity was first documented for CBP21, a CBM33 secreted by the chitinolytic bacterium *Serratia marcescens*, which previously had been shown to boost chitin depolymerization by chitinases (9). CBP21 catalyzes oxidative cleavage of the β-1,4 glycosidic bonds that results in oxidation of the C1 carbon (5). The reaction involves molecular oxygen, an external electron donor, and a metal that is coordinated by the two conserved histidines (Fig. 1). The identity of the metal was not disclosed in early work (5, 10), but functional studies on related enzymes, a CBM33 from *Enterococcus faecalis* (11) and three GH61s (4, 12, 13), have later indicated that the LPMOs are copper-dependent enzymes. However, because of several complications, such as the indiscriminate nature of the metal binding site (see below) and the fact that the CBM33 crystal structures obtained so far mostly were metal-free, many aspects of metal binding remain unresolved. Even less is known about how these enzymes, with their unique flat binding surfaces devoid of traditional substrate binding grooves or pockets, interact with the substrate. Nothing is known about dynamics in these remarkably compact proteins.

Here, we describe the solution structure of CBP21 determined by NMR spectroscopy. Both NMR and isothermal titration calorimetry (ITC) were used to investigate metal binding and its pH dependence. Furthermore, we studied the molecular basis of cyanide inhibition as well as protein dynamics. Finally, by applying an NMR-based approach that exploits the pH dependency of substrate binding, we were able to directly map the substrate binding surface of CBP21. Thus, we provide important insights into fundamental properties underlying the unprecedented and unresolved catalytic mechanism of these recently discovered enzymes.

Results

CBP21 Structure. The solution structure of CBP21 (Fig. 1*A* and Table S1) (Protein Data Bank ID code 2LHS) was calculated based on 4,330 NOE-derived geometrical constraints, 231 TALOS+ (14) -derived dihedral angles restraints, and two disulphide bridges (8) (Cys41-Cys49 and Cys135-Cys162). The CBP21 core structure is formed by a distorted β-sandwich consisting of nine antiparallel and one parallel β-strands. The exterior of the protein

Author contributions: F.L.A., M.S., G.S.-B., V.G.H.E., and G.V.-K. designed research; F.L.A., M.S., and G.V.-K. performed research; F.L.A., M.S., G.S.-B., V.G.H.E., and G.V.-K. analyzed data; and F.L.A., M.S., G.S.-B., V.G.H.E., and G.V.-K. wrote the paper.

The authors declare no conflict of interest.

This article is a PNAS Direct Submission.

Data deposition: The NMR, atomic coordinates, chemical shifts, and restraints have been deposited in the Protein Data Bank, www.pdb.org (PDB ID code 2LHS).

[1]To whom correspondence may be addressed. E-mail: finn.l.aachmann@ntnu.no or gustko@umb.no.

This article contains supporting information online at www.pnas.org/lookup/suppl/doi:10.1073/pnas.1208822109/-/DCSupplemental.

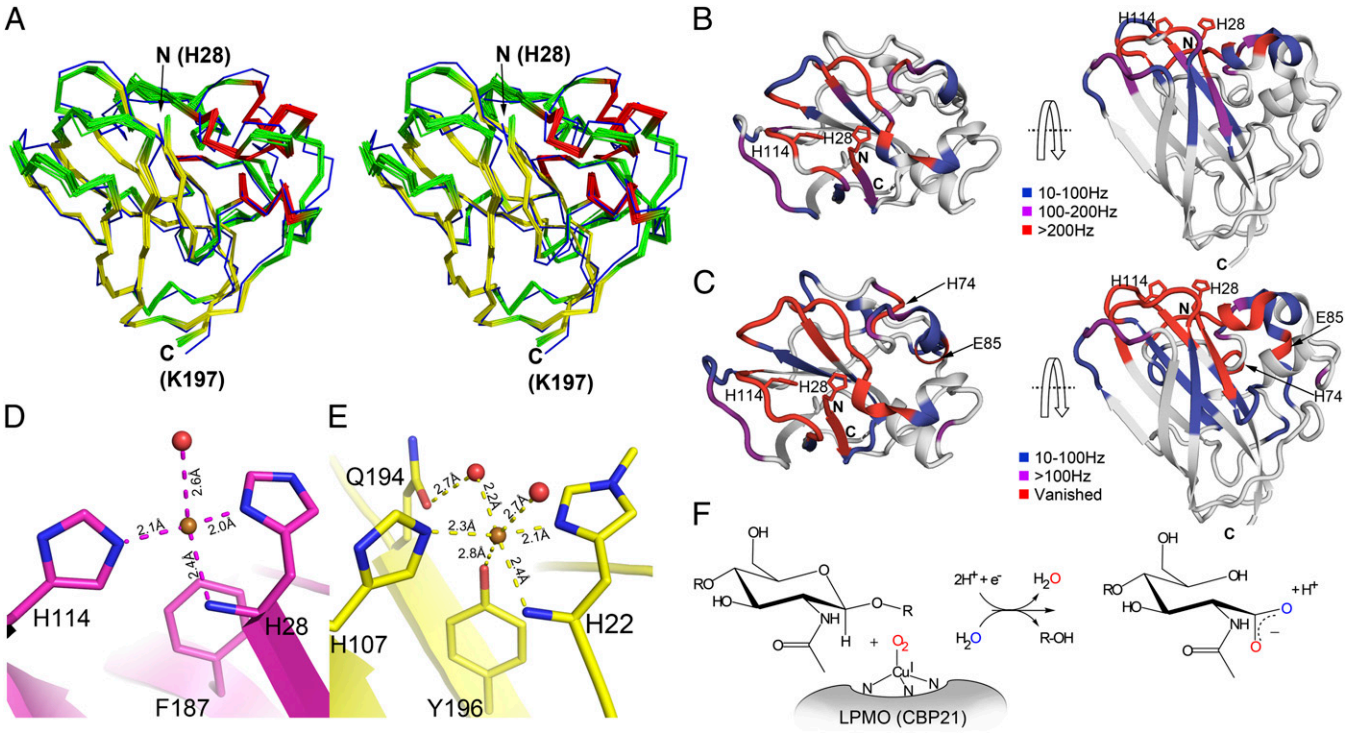

Fig. 1. Structure of CBP21 and metal ion binding. (*A*) Stereo image showing a superposition of the X-ray crystallographic structure of CBP21 (Protein Data Bank ID code 2BEM; blue) and the 20 energy-minimized conformations of CBP21 solved by solution NMR (Protein Data Bank ID code 2LHS) colored red (helix), yellow (strand), and green (coil). The N- and C-terminal residues are indicated (note that the N terminus is part of the catalytic center). The mean rmsd between the X-ray crystallographic structure and the 20 NMR structures was calculated to be 1.54 ± 0.07 Å using the Swiss-Pdb Viewer software. (*B* and *C*) Change in amino acid chemical shifts (^{15}N and ^{13}C HSQC) on adding 2.0 mM Zn^{2+} (*B*) or Cu^{2+} (*C*) to 0.5 mM $CBP21_{apo}$, where the degree of change is indicated by the coloring scheme. The CBP21 structure is shown by a top view (*Left*) and side view (*Right*). The signals of residues in close proximity to the Cu^{2+} ion vanish because of the paramagnetic relaxation enhancement (PRE) effect induced by Cu^{2+}. The data for copper (*C*) also indicated a secondary metal binding site comprising (nonconserved) residues Glu85 and His74 that showed weak and ambiguous interactions. These interactions were only observable at the highest tested Cu^{2+} concentration (2 mM) and thus, regarded as artifacts. (*D* and *E*) Metal binding sites observed in the crystal structures of CBP21 (*D*; with an unknown metal ion bound) (8) and *Ta*GH61A (*E*; with copper bound) (12). Metal ions and water molecules are shown as bronze and red colored spheres, respectively. Residue numbering is based on the explicit sequence (i.e., the signal sequence is taken into account; 27 residues for CBP21 and 21 residues for *Ta*GH61A; H28 and H22 are the N-terminal residues, respectively). Note that *Ta*GH61A H22 is posttranslationally methylated at Nε2 (*E*) (12). Structure illustrations were prepared using PyMOL (30). (*F*) Schematic overview of the reaction catalyzed by LPMOs based on existing experimental evidence. The LPMO, coordinating a reduced copper ion [Cu(I)], activates molecular oxygen that, through an unknown reaction mechanism, results in cleavage of the glycosidic bond, oxidation of the C1 carbon by a single oxygen (red oxygen), and hydrolysis (blue oxygen) to yield the aldonic acid end product. Ref. 4 discusses additional suggestions concerning the mechanism. Note that copper binding involves three nitrogen atoms, as indicated, namely the N-terminal amino group and an imidazole nitrogen in each of the two conserved histidines.

is decorated with one short α-helix, four short 3^{10}-helix segments, and several ordered loops. Fig. 1*A* shows that the solution structure of CBP21 is highly similar to the X-ray crystallographic structure (8); there are, however, minor differences in a solvent-exposed area of the enzyme that is involved in substrate binding (discussed below).

Metal Binding. Interaction of CBP21 with divalent metals was probed by recording changes in chemical shifts in ^{15}N heteronuclear single quantum coherence (HSQC) spectra upon titration with Ca^{2+}, Mg^{2+}, Fe^{3+}, Co^{2+}, Zn^{2+}, or Cu^{2+} ions (Fig. 1 *B* and *C* and Fig. S1). All ions showed binding to an interaction site located between His28 and His114, where the side chains of both residues and the N-terminal amino group of His28 coordinate the metal ion (Fig. 1*D*) (it should be noted that the N-terminal leader peptide is taken into account when numbering the amino acids of CBP21; His28 is the N-terminal residue of the mature protein). Based on these experiments, the dissociation constants (K_d values) for the various metals were estimated to have the following order: $Ca^{2+} > Mg^{2+} > Fe^{3+} > Co^{2+} >> Zn^{2+} > Cu^{2+}$, varying from > 10 mM for Ca^{2+} to < 0.5 mM for Co^{2+} and substantially lower for Zn^{2+} and Cu^{2+} (Fig. S1).

Considering the involvement of histidines in metal binding, ^{13}C HSQC spectra of the aromatic region were recorded in the absence and presence of Zn^{2+}, Cu^{2+}, or Cu^{1+}. For Zn^{2+} titration, new peaks for His28- and His114-coordinating Zn^{2+} appeared and increased in intensity upon titration (Fig. 2*A*). The titrations showed strong binding of Zn^{2+} and indicated a K_d in a concentration range (lower than micromolar) that is too low for determination by NMR. Obtaining K_d values for the binding of Cu^{2+} was impossible because of the paramagnetic properties of Cu^{2+} that lead to broadening of the NMR signals of residues within ∼10 Å from the copper binding site to levels beyond detection (15). However, a competition experiment clearly showed that Cu^{2+} binds more tightly than Zn^{2+} (Fig. 2*B*). On titration of metal-free CBP21 with Cu^{2+}, the signal for both histidines disappeared at a 1:1 molar ratio between protein and the metal ion (Fig. 2*D*). Competition experiments also showed that Cu^{1+} binds more strongly than Zn^{2+} (Fig. 2*C*) and Cu^{2+} (Fig. 2*E*).

Because the K_d values were too low to be precisely determined from the NMR data, ITC experiments were conducted to obtain more accurate data. Because of the low solubility of Cu^{1+}, only dissociation constants for Zn^{2+} and Cu^{2+} were determined at 330 and 55 nM, respectively (Fig. 3 and Table 1). In agreement with

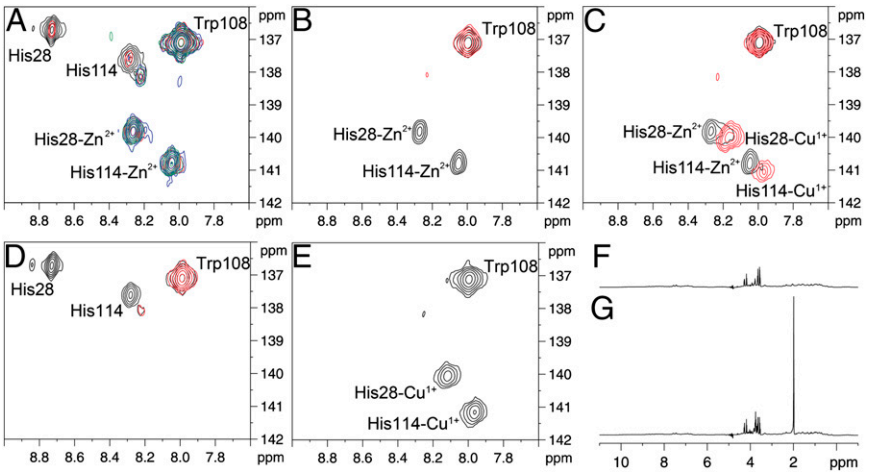

Fig. 2. Spectral changes in CBP21 on interaction with zinc and copper ions. (*A*) Overlay of ^{13}C HQSC spectra for 0.5 mM CPB21 in the presence of 0 (black), 0.25 (red), 0.50 (blue), and 2.0 (green) mM Zn^{2+}. New signals appear for His28 and His114 on binding of Zn^{2+} and increase in intensity on titration, displaying a slow exchange situation. This result indicates that both histidines have high affinity for Zn^{2+}. The signal for Trp108, a residue not affected by metal binding, is the same in all spectra. (*B*) Overlay of ^{13}C-HQSC spectra for 0.5 mM CBP21 and 1 mM Zn^{2+} in the presence (red) or absence (black) of 0.5 mM Cu^{2+}. On binding of Cu^{2+} ions, the signals for the metal binding site (His28 and His114) broaden beyond detection because of PRE. The absence of red signals, thus, shows that Cu^{2+} binds stronger than Zn^{2+}. (*C*) Overlay of ^{13}C HQSC spectra for 0.5 mM CBP21 and 1 mM Zn^{2+} in the presence (red) or absence (black) of ~0.65 mM Cu^{1+} under reducing conditions. Because Cu^{1+} is not paramagnetic, signals for His28 and His114 are still present in the spectrum. (*D*) Overlayed ^{13}C HQSC spectra for 0.5 mM metal-free CBP21 in the presence (red) or absence (black) of 0.5 mM Cu^{2+}. Binding of copper eliminates His28 and His114 signals caused by PRE. (*E*) ^{13}C HQSC spectrum for 0.5 mM CBP21 in the presence of 0.5 mM Cu^{1+} and 5.0 mM Cu^{2+} in anaerobic conditions. This spectrum shows that Cu^{1+} bound to CBP21 is not oxidized or replaced by free Cu^{2+}, because line broadening effects (PRE) of the His28 and His114 signals are not observed. The presence (*F*) or absence (*G*) of Cu^{2+} in solution is verified by the proton spectrum, where a high concentration of Cu^{2+} ions results in generally enhanced relaxation conditions in the sample (e.g., leading to disappearance of the acetate signal at ~1.9 ppm).

the NMR data, this result showed that CBP21 had higher affinity for Cu^{2+} than Zn^{2+} (sixfold). The K_d for Cu^{1+} binding can be obtained by combining, in a thermodynamic cycle, the energetics of Cu^{2+} dissociation from CBP21 and the electron transfer reaction between aqueous Cu^{2+} and CBP21-Cu^{1+} (Fig. S2). The latter was obtained by experimentally determining the equilibrium constant between CBP21-Cu^{2+} and a suitable electron transfer mediator (*N,N,N′,N′*-tetramethyl-1,4-phenylenediamine; TMP) (16). The $E°$ for the equilibrium, TMPred + CBP21-Cu^{2+} ⇄ TMPox + CBP21-Cu^{1+}, was determined to be 2 mV (Fig. S2, I). Subtraction of the $E°$ for the TMP_{ox}/TMP_{red} redox couple yields an $E°$ of 275 mV for the CBP21-Cu(II)/CBP21-Cu(I) redox couple, a value that is 115 mV higher than the value of aqueous Cu^{2+}/Cu^{1+} (Fig. S2, II). Because the values are related according to the thermodynamic cycle depicted in Fig. S2, the 115-mV increase in redox potential reflects tighter binding of Cu^{1+} relative to Cu^{2+} and leads to a calculated K_d for Cu^{1+} of 1.2 nM (Fig. S2, III). Notably, this value should be considered an estimate, particularly because the thermodynamic values used in the cycle, because of technical limitations, had to be determined at slightly different temperatures (varying from 6 °C to 25 °C).

To illustrate the functional implications of these findings, and exploiting a method for generating metal-free CBP21 ($CBP21_{apo}$; by reduction in pH, see below), we examined the enzymatic activity of $CBP21_{apo}$ in the presence of a metal chelator (EDTA) and various added metal ions. The data clearly show that Cu^{2+} is the only one of the tested divalent metals that is able to reactivate metal-free (and completely inactive) $CBP21_{apo}$ (Fig. 4 and Fig. S3).

Cyanide Inhibition. Cyanide inhibits CBP21 (5), most likely because it is a dioxygen mimic. Addition of sodium cyanide to CBP21-Zn^{2+} resulted in substantial chemical shifts for His28 and His114 in both ^{15}N and ^{13}C HSQC NMR spectra (Fig. S4), whereas only limited changes were observed for other residues. [Because of the paramagnetic properties of Cu^{2+} (not visible in NMR experiments) and the experimental challenges in working with Cu^{1+} (low solubility), Zn^{2+} was chosen as the metal ligand.] In a control experiment where $CBP21_{apo}$ was incubated with cyanide, no changes were observed for either the ^{15}N or ^{13}C HSQC NMR spectra, indicating that the effect of cyanide is highly local, which would be the case if this oxygen mimic binds directly to the metal ion.

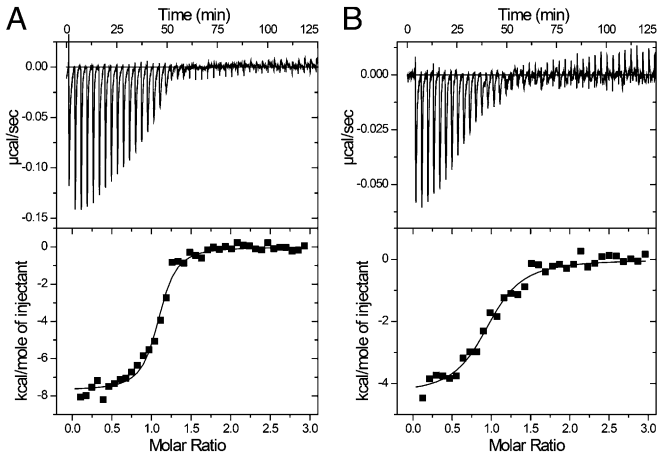

Fig. 3. Thermograms (*Upper*) and binding isotherms with theoretical fits (*Lower*) obtained for the binding of 150 µM Cu^{2+} (*A*) or Zn^{2+} (*B*) to 5 µM $CBP21_{apo}$ at 6 °C.

pH Titrations. By acid titration of $CBP21_{apo}$, the pK_a values of His28 and His114 were determined to be 7.03 ± 0.25 and 5.85 ± 0.09, respectively (Fig. 5 *A* and *B*), which are common values for histidines in proteins (17). In the presence of Zn^{2+}, both histidine residues first started to titrate below pH 5.0 and were fully protonated at pH 4.0 (Fig. 5*C*). The degree of protonation was calculated based on the integrals for the His-Zn^{2+} and His-H^+ peaks, and this finding indicated that both histidines have a pK_a

Table 1. Thermodynamic parameters for binding of 150 µM Cu^{2+} or Zn^{2+} to 5 µM $CBP21_{apo}$ at t = 6 °C in 20 mM Pipes (pH 6.5)

Metal ion	K_d*	$\Delta G^{\dagger}$	$\Delta H^{\dagger}$	$-T\Delta S^{\dagger}$
Cu^{2+}	55 ± 8	−9.3 ± 0.2	−7.5 ± 0.2	−1.8 ± 0.3
Zn^{2+}	330 ± 40	−8.3 ± 0.1	−3.9 ± 0.2	−4.4 ± 0.2

*Nanomolar.
†Kilocalorie per mole.

BIOCHEMISTRY

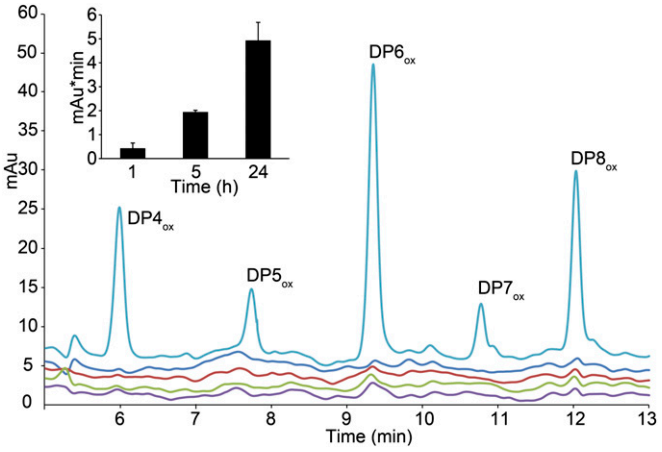

Fig. 4. Cu^{2+} reactivation of CBP21. Chromatographic analysis of soluble products obtained on incubating 2.0 μM metal-free CBP21 with 2.5 mg/mL β-chitin fibers in the presence of 1.0 mM ascorbic acid, 50 μM EDTA, and 25 μM $CuSO_4$ (light blue), $ZnSO_4$ (dark blue), $MgSO_4$ (red), $MnSO_4$ (green), or buffer (control; purple) at 37 °C in 20 mM Tris·HCl (pH 8.0) for 24 h. *Inset* shows formation of $(GlcNAc)_5GlcNAc$-aldonic acid ($DP6_{ox}$) over time by CBP21-Cu^{2+}. Additional details on product analysis are in Fig. S3.

between 4.3 and 4.4. Both histidines first started to exchange Cu^{1+} with protons below pH 4.7 and were fully protonated first at pH 2.9 (Fig. 5*D*), with pK_a values of 3.3–3.5 and 3.5–3.7 for His28 and His114, respectively.

Altogether, the pK_a perturbations of the histidines by the metal ions clearly show that Cu^{1+} binds stronger that Zn^{2+} and that the enzyme is in its apo form at pH < 2.9.

The variation in pK_a perturbations will, to a certain extent, reflect the difference in binding strength of Cu^{1+} vs. Zn^{2+}, and this result may be used to estimate the K_d for Cu^{1+}. The observed differences in the pK_a perturbations exerted by Cu^{1+} compared with Zn^{2+} correspond to a total free energy change ($\Delta G_r°$) of 2.3 kcal/mol (1.0 kcal/mol for His28 and 1.3 kcal/mol for His114; calculated by using $\Delta G_r° = -RT \ln K$). Adding this free energy change to the free energy change of Zn^{2+} binding (8.3 kcal/mol; from ITC data) (Table 1) yields a $\Delta G_r°$ of 10.6 kcal/mol, corresponding to a K_d value of 16 nM. This calculation is based on the rather unlikely assumption that 100% of the binding free energy is reflected in the measured pK_a values, and thus, the value of 16 nM represents an upper limit rather than the real value. The upper limit of 16 nM for the K_d for Cu^{1+} is lower than the K_d for Cu^{2+} determined with ITC (55 nM), and it is compatible with the K_d value for Cu^{1+} obtained using the thermodynamic cycle described above (1.2 nM).

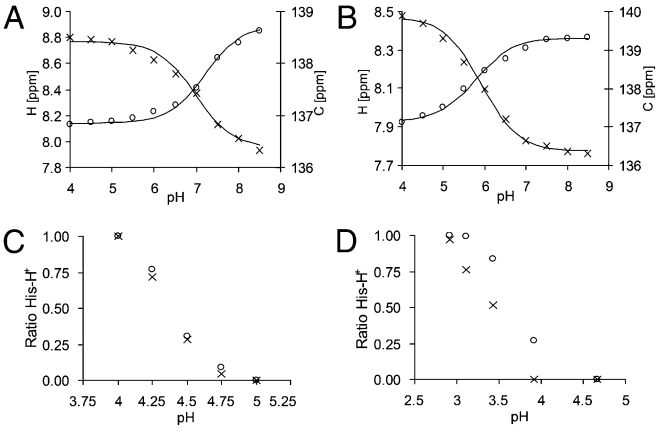

Fig. 5. Titration of His28 and His114 (^{13}C HSQC spectra). Chemical shifts of $C^{\varepsilon 1}$ (○) and $H^{\varepsilon 1}$ (×) are plotted as a function of pH (4.0–8.5) for His28 (*A*) and His114 (*B*) for $CP21_{apo}$. The data were fitted to the Henderson–Hasselbach equation (fitted curve indicated by lines), yielding pK_a values 7.03 ± 0.25 and 5.85 ± 0.09 for His28 and His114, respectively. (*C* and *D*) Ratio of protonated histidine vs. metal bound histidine during a similar titration for CBP21 saturated with Zn^{2+} and Cu^{1+}, respectively. In the presence of Cu^{1+}, pK_a values are 3.3–3.5 for His28 (×) and 3.5–3.7 for His114 (○). In the presence of Zn^{2+}, both residues have a pK_a of 4.3–4.4.

Mobility Studies. The CPB21 metal binding site is able to accommodate a range of metal ions, which indicates a flexible metal binding site. To gain insight into this issue, $^{15}N\{H\}$-NOEs as well as T_1 and T_2 relaxation times (picosecond and nanosecond timescales) were measured in the presence or absence of Zn^{2+}.

Both the $^{15}N\{H\}$-NOEs and relaxation data are relatively featureless and show the characteristics of a rigid protein. The one clear exception is the N terminus of the protein, which shows increased flexibility in the absence of metal ions (Fig. S5). However, in the presence of the metal ion, this extra flexibility at the N terminus is lost.

Substrate Binding. Amino acid residues involved in binding to chitin were mapped using an NMR approach that exploits the pH dependency of substrate binding (Fig. S6) in a $^2H/^1H$ exchange experiment with nanofibrillar β-chitin. Fig. 6*A* shows that chitin binding protected two regions from exchange, Gln53-Ser58 and Leu110-Thr116, providing direct experimental evidence that these surface-exposed regions are involved in substrate binding (Fig. 6 *B–D*).

The correlation between pH-dependent desorption of CBP21 from chitin (pH 3–4) (Fig. S6) and the observed loss of the metal cofactor (at a pH of ~3, depending on the metal and its redox state; see above) prompted us to attempt desorbing CBP21 from chitin with a metal chelator only (EDTA). This process was successful at 200 mM EDTA, providing a useful alternative purification protocol (Fig. S7).

Discussion

Considering the dominance of LPMOs in the secretomes of biomass-degrading microorganisms (18), the abundance of LPMO-encoding genes in such organisms, and the documented beneficial effects of LPMOs on biomass conversion, it seems that we have only seen the beginning of what may be a very important development in enzymatic biomass refining. Many important aspects of these recently discovered enzymes remain unresolved, including the catalytic mechanism and the structural determinants of substrate specificity. The NMR and ITC studies described above provide unprecedented insight into several key properties of these enzymes.

The data presented in this study unambiguously show that CBP21 is a copper-dependent LPMO. Cu^{2+} binds CBP21with nanomolar affinity (Figs. 2 and 3 and Table 1) and is essential for catalysis (Fig. 4). Binding of cyanide, a di-oxygen mimic and potent inhibitor of CBP21, to the metal (Fig. S4) indicates that the metal ion is actively involved in oxidative cleavage of the substrate by CBP21. Importantly, the redox potential of the Cu^{2+}/Cu^{1+} couple in CBP21 is elevated relative to the redox potential of aqueous Cu^{2+}/Cu^{1+} (115 mV), which reflects tighter binding of Cu^{1+} relative to Cu^{2+}. Tighter binding of Cu^{1+} is confirmed by the competition experiments in anaerobic conditions, which showed that CBP21-Cu^{1+} was not oxidized by a 10-fold surplus of Cu^{2+} in the solution (Fig. 2*E*). The 115-mV increase in redox potential is in accordance with previous studies, showing that complexation of Cu^{2+} in a type 2 copper binding site increases the redox potential by 40–240 mV relative to the potential of aqueous Cu^{2+} (19–21). The fact that CBP21 seems to preferably bind Cu^{1+} coincides with the notion that molecular oxygen tends to bind

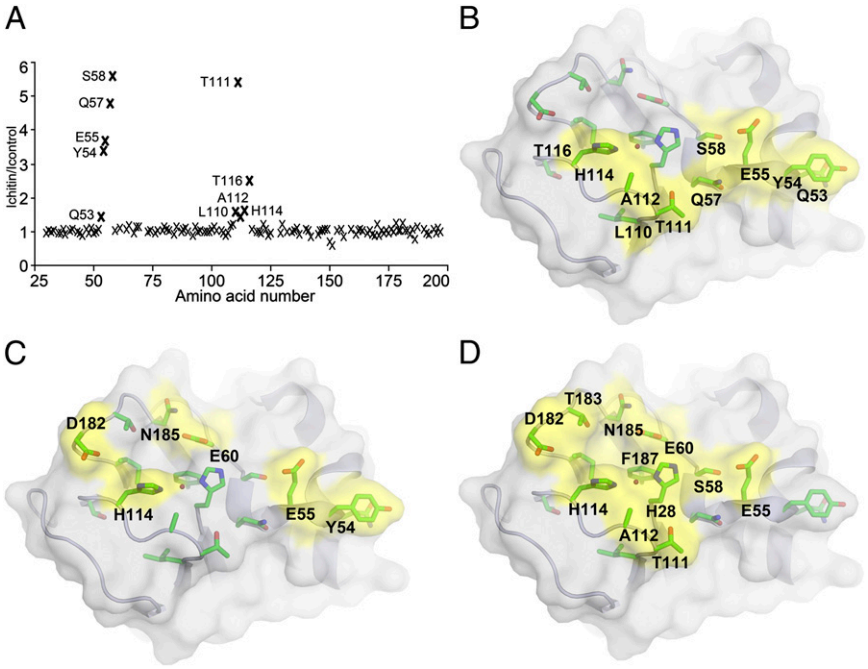

Fig. 6. Chitin binding by CBP21. (*A*) Signal intensities in ^{15}N HSQC spectra of CBP21 in the presence of chitin divided by their intensities in the absence of chitin after deuterium (^{2}H) exchange in buffer (10 mM phosphate buffer, pH 6.0, 10 mM NaCl) for 30 min. Exchange was quenched by reducing the pH to 3.5 (using 50 mM acetate buffer). Although most signal intensity ratios are close to one, some amino acids (labeled) show higher values owing to significant protection of the backbone amide proton against exchange in the presence of chitin, presumably by chitin binding. (*B*) Residues identified as involved in chitin binding from the data in *A* mapped on the surface of CBP21 by yellow surface coloring. (*C*). Residues involved in chitin binding by CBP21 as determined by site-directed mutagenesis in a previous study (8) shown by yellow surface coloring. (*D*) Highly conserved residues on the CBP21 substrate binding surface determined by sequence analysis available in the ConSurf database (31) shown by yellow surface coloring. The database entry used was Protein Data Bank ID code 2BEM. Residues scoring more than eight were considered highly conserved (9, maximum; 1, minimum).

copper proteins in their reduced monovalent state (22). These data and considerations are compatible with the initial steps of a catalytic mechanism proposed for a GH61-type LPMO in the work by Phillips et al. (4): Cu^{2+} is reduced on the enzyme to Cu^{1+} by an electron supplied by a chemical compound or an enzyme, such as cellobiose dehydrogenase; on oxygen binding to the metal ion, the electron is transferred to generate a superoxo intermediate (Fig. 1*F*).

Notably, the mapping of enzyme–substrate interactions unequivocally shows that the metal binding site is in direct proximity to the substrate when CBP21 is bound to the chitin surface (Fig. 6).

Although CBM33-type and GH61-type LPMOs seem to catalyze essentially the same reaction (4, 5, 12, 13, 23) and have similar active sites (Fig. 1 *D* and *E*), their metal binding sites do show some notable differences. The work by Quinlan et al. (12) indicated that the K_d for Cu^{2+} binding to *Ta*GH61A is below 1 nM, suggesting that the binding affinity is at least 50-fold higher than the binding affinity for CBP21. In CBP21, Cu^{2+} is coordinated by two histidines, whereas *Ta*GH61A and other GH61s have a tyrosine that contributes to ion coordination through the hydroxyl group and a glutamine that indirectly contributes to metal coordination through positioning a water molecule that interacts with the copper ion (Fig. 1*E*). Moreover, the N-terminal histidine is methylated in all structures so far published for GH61 enzymes (12). This modification may increase the affinity for the metal ion, because 3-methyl histidine has a pK_a elevated by ∼0.5 compared with a normal histidine (24). Alternatively, the methylation may have favorable structural/dynamic effects, such as prepositioning the N-terminal histidine to optimally accommodate the copper ion. Notably, differences between the binding sites are also illustrated by the fact that no other metals than copper ions were found to bind to *Ta*GH61A (12), whereas CBP21 binds Zn^{2+} with low micromolar affinity.

Interestingly, Cu^{1+} dissociates from His28 and His114 at pH values that are also known to induce dissociation of substrate-bound CBP21 [β-chitin (Fig. S6) and regenerated chitin (ref. 25)]. Although this finding suggests that substrate binding depends on the presence of a bound metal ion, it should be noted that the EDTA concentrations needed to elute CBP21 from a chitin column were much higher than those concentrations needed for completely inactivating the enzyme. Thus, metal depletion alone is insufficient for elution, and other interactions do contribute to binding (which was also suggested by the early mutagenesis work described in ref. 8).

Obtaining information on LPMO–substrate interactions is challenging because of the biphasic nature of the experimental system (solid substrate and soluble enzyme). Using an approach that exploits the pH dependency of both the chitin–CBP21 interaction and the ^{2}H/^{1}H exchange rate, we were able to directly identify residues involved in binding CBP21 to the chitin surface (Fig. 6). Identified residues matched with residues previously suggested to be involved in substrate binding based on combined structure and sequence analysis and mutagenesis (8), and they included the only solvent-exposed aromatic amino acid in the previously proposed binding area, Tyr54 (Fig. 6) (8). Interestingly, the identified binding residues line up in a narrow stretch along the substrate binding surface that could match the width of a single polysaccharide chain (Fig. 6*B*). It is important to note, however, that the ^{2}H/^{1}H exchange experiments reflect protection of amide protons and that it is conceivable that certain residues interact with chitin without their amide protons being protected from rapid exchange (the presence of additional interacting residues is suggested by mutagenesis and sequence conservation data; Fig. 6 *C* and *D*). CBP21 does not bind single chitin chains but rather, an ordered array of chains (like the crystalline surface of a chitin fibril) (26). Therefore, if there really would be only a narrow stretch of interacting residues, one might speculate that the protein that binds with this stretch is oriented perpendicularly to the polysaccharide chains. Interestingly, a similar (speculative) suggestion has very recently been made on the bases of the crystal structure of a GH61 protein (27).

Despite the availability of nine LPMO crystal structures (four CBM33 structures and five GH61 structures), most aspects of these enzymes' intriguing catalytic activity have remained unknown. The first NMR structure of an LPMO described here has allowed the study of several functional aspects. Finally, because molecular motion and NMR share the same timescale, we also obtained dynamic information about the protein. The results show generally very little flexibility, with the exception of the metal binding site, which in the absence of a metal ion, shows some

highly local flexibility. We conclude that the unique ability of LPMOs to oxidatively cleave polysaccharide chains without expelling these chains from their crystalline context depends on a fixed geometry around the oxygen-coordinating metal binding site. The rigid nature of CBP21 seems well-adapted to bind the highly ordered crystalline chitin surface.

Materials and Methods

Details are in SI Materials and Methods.

NMR Spectroscopy. Isotope-labeled recombinant CBP21 used in NMR experiments was produced in *Escherichia coli* cultivated in isotope-enriched (^{15}N or $^{13}C,^{15}N$) M9 minimal medium and purified as described in ref. 8. NMR assignment of CBP21 was done previously (28), and NMR data for CBP21 were obtained using a Bruker Avance 600-MHz spectrometer.

Detection of residues involved in binding of CBP21 to chitin was accomplished with a method that exploits the pH dependency of binding. The method involved binding CBP21 to β-chitin in buffered H_2O followed by buffer exchange to D_2O at pH 6.0. At this stage, backbone amide groups shielded from solvent by binding to chitin will retain their protons, whereas amide protons on solvent exposed parts of the enzyme are exchanged with deuterium. CBP21 was then released from the substrate by pelleting the CBP21-bound chitin by centrifugation and resuspension in H_2O buffered to pH 3.5. At this pH, proton exchange is slow ($k_{exchange} \sim 0.25 \times 10^{-3}$ s^{-1}), and the concomitantly recorded ^{15}N HSQC spectrum clearly revealed backbone amide groups having protons bound (giving very intense signals) vs. deuterium bound (giving weak signals). By comparing the two spectra, residues involved in binding could be identified by evaluating the backbone amide group intensity differences. Details are in SI Materials and Methods.

Enzyme Activity and Binding Assays. CBP21 was produced in the apo form by chitin affinity chromatography (8) using 0.2 M EDTA to elute the protein. Metal dependency of CBP21 activity was assayed by incubating $CBP21_{apo}$ in the presence of 2.5 mg/mL β-chitin fibers [produced according to the method described in the work by Fan et al. (29)], 1.0 mM ascorbic acid (electron donor), 50 μM EDTA, and 25 μM metal ion salt in 20 mM Tris·HCl (pH 8.0) at 37 °C. Soluble products were analyzed at 1, 5, and 24 h incubation using hydrophobic interaction liquid chromatography-based chromatographic methods and MALDI-TOF MS analysis as described previously (5).

Details are in SI Materials and Methods.

ITC. Dissociation constants and thermodynamic data for binding of Zn^{2+} and Cu^{2+} to CBP21 was achieved by measuring the heat produced when injecting 4-μL aliquots (40 in total) of 150 μM metal ion solutions into the reaction cell of a VP-ITC system from MicroCal containing 1.42 mL 5 μM $CBP21_{apo}$ solution buffered to pH 6.5 with Pipes at 6 °C. Details are in SI Materials and Methods.

Redox Potential Determination. Determination of the cell potential ($E°$) for the CBP21-Cu^{2+}/CBP21-Cu^{1+} redox couple was done by allowing reduced TMP (50 μL and 300 μM) to react with CBP21-Cu^{2+} (50 μL and 70 μM) and reach equilibrium under anaerobic conditions, and the extent of reaction and hence, the equilibrium constant, were determined by measuring absorbance from the formed TMP radical cation at 610 nm. The equilibrium constant was used to calculate $E°$ for the CBP21-Cu^{2+}/CBP21-Cu^{1+} redox couple, because this result is proportional to the difference in the cell potentials between the two redox couples in the electron transfer reaction. Details are in SI Materials and Methods.

ACKNOWLEDGMENTS. We thank Anne Cathrine Bunæs for assisting with protein purification and Reinhard Wimmer for assisting with TALOS+ and energy refinement. This work was funded by Norwegian Research Council (NFR) Grants 182695/I40 (to F.L.A. and G.S.-B.), 209335/F20 (to M.S.), 186946 (to V.G.H.E. and G.V.-K.), 196885 (to V.G.H.E. and G.V.-K.), and 214138 (to G.V.-K.).

1. Henrissat B, Driguez H, Viet C, Schulein M (1985) Synergism of cellulases from *Trichoderma-reesei* in the degradation of cellulose. *Bio-Technol* 3:722–726.
2. Merino ST, Cherry J (2007) Progress and challenges in enzyme development for biomass utilization. *Adv Biochem Eng Biotechnol* 108:95–120.
3. Mba Medie F, Davies GJ, Drancourt M, Henrissat B (2012) Genome analyses highlight the different biological roles of cellulases. *Nat Rev Microbiol* 10(3):227–234.
4. Phillips CM, Beeson WT, Cate JH, Marletta MA (2011) Cellobiose dehydrogenase and a copper-dependent polysaccharide monooxygenase potentiate cellulose degradation by *Neurospora crassa*. *ACS Chem Biol* 6(12):1399–1406.
5. Vaaje-Kolstad G, et al. (2010) An oxidative enzyme boosting the enzymatic conversion of recalcitrant polysaccharides. *Science* 330(6001):219–222.
6. Cantarel BL, et al. (2009) The Carbohydrate-Active EnZymes database (CAZy): An expert resource for Glycogenomics. *Nucleic Acids Res* 37(Database issue):D233–D238.
7. Karkehabadi S, et al. (2008) The first structure of a glycoside hydrolase family 61 member, Cel61B from Hypocrea jecorina, at 1.6 A resolution. *J Mol Biol* 383(1):144–154.
8. Vaaje-Kolstad G, Houston DR, Riemen AHK, Eijsink VGH, van Aalten DMF (2005) Crystal structure and binding properties of the *Serratia marcescens* chitin-binding protein CBP21. *J Biol Chem* 280(12):11313–11319.
9. Vaaje-Kolstad G, Horn SJ, van Aalten DMF, Synstad B, Eijsink VGH (2005) The non-catalytic chitin-binding protein CBP21 from *Serratia marcescens* is essential for chitin degradation. *J Biol Chem* 280(31):28492–28497.
10. Harris PV, et al. (2010) Stimulation of lignocellulosic biomass hydrolysis by proteins of glycoside hydrolase family 61: Structure and function of a large, enigmatic family. *Biochemistry* 49(15):3305–3316.
11. Vaaje-Kolstad G, et al. (2012) Characterization of the chitinolytic machinery of *Enterococcus faecalis* V583 and high-resolution structure of its oxidative CBM33 enzyme. *J Mol Biol* 416(2):239–254.
12. Quinlan RJ, et al. (2011) Insights into the oxidative degradation of cellulose by a copper metalloenzyme that exploits biomass components. *Proc Natl Acad Sci USA* 108(37):15079–15084.
13. Westereng B, et al. (2011) The putative endoglucanase PcGH61D from *Phanerochaete chrysosporium* is a metal-dependent oxidative enzyme that cleaves cellulose. *PLoS One* 6(11):e27807.
14. Shen Y, Delaglio F, Cornilescu G, Bax A (2009) TALOS+: A hybrid method for predicting protein backbone torsion angles from NMR chemical shifts. *J Biomol NMR* 44(4):213–223.
15. Arnesano F, Banci L, Bertini I, Thompsett AR (2002) Solution structure of CopC: A cupredoxin-like protein involved in copper homeostasis. *Structure* 10(10):1337–1347.
16. Sørlie M, Seefeldt LC, Parker VD (2000) Use of stopped-flow spectrophotometry to establish midpoint potentials for redox proteins. *Anal Biochem* 287(1):118–125.
17. Creighton TE (1997) *Proteins: Structure and Molecular Properties* (Freeman, New York), 2nd Ed, pp 407–410.
18. Znameroski EA, et al. (2012) Induction of lignocellulose-degrading enzymes in *Neurospora crassa* by cellodextrins. *Proc Natl Acad Sci USA* 109(16):6012–6017.
19. Jacobson F, et al. (2007) pH dependence of copper geometry, reduction potential, and nitrite affinity in nitrite reductase. *J Biol Chem* 282(9):6347–6355.
20. Ljones T, et al. (1978) Dopamine β-monooxygenase: Electron paramagnetic resonance and oxidation—reduction properties of the enzyme-bound copper. *FEBS Lett* 92(1):81–84.
21. Rae TD, Schmidt PJ, Pufahl RA, Culotta VC, O'Halloran TV (1999) Undetectable intracellular free copper: The requirement of a copper chaperone for superoxide dismutase. *Science* 284(5415):805–808.
22. Que L, Jr., Tolman WB (2008) Biologically inspired oxidation catalysis. *Nature* 455(7211):333–340.
23. Forsberg Z, et al. (2011) Cleavage of cellulose by a CBM33 protein. *Protein Sci* 20(9):1479–1483.
24. Paiva ACM, Juliano L, Boschcov P (1976) Ionization of methyl derivatives of imidazole, histidine, thyreotropin releasing factor, and related compounds. *J Am Chem Soc* 98(24):7645–7648.
25. Suzuki K, Suzuki M, Taiyoji M, Nikaidou N, Watanabe T (1998) Chitin binding protein (CBP21) in the culture supernatant of *Serratia marcescens* 2170. *Biosci Biotechnol Biochem* 62(1):128–135.
26. Nishiyama Y, Noishiki Y, Wada M (2011) X-ray structure of anhydrous beta-chitin at 1 angstrom resolution. *Macromolecules* 44:950–957.
27. Li X, Beeson WT, 4th, Phillips CM, Marletta MA, Cate JHD (2012) Structural basis for substrate targeting and catalysis by fungal polysaccharide monooxygenases. *Structure* 20(6):1051–1061.
28. Aachmann FL, Eijsink VGH, Vaaje-Kolstad G (2011) 1H, 13C, 15N resonance assignment of the chitin-binding protein CBP21 from Serratia marcescens. *Biomol NMR Assign* 5(1):117–119.
29. Fan Y, Saito T, Isogai A (2008) Preparation of chitin nanofibers from squid pen beta-chitin by simple mechanical treatment under acid conditions. *Biomacromolecules* 9(7):1919–1923.
30. DeLano WL, Lam JW (2005) PyMOL: A communications tool for computational models. *Abstr Pap Am Chem S* 230:1371–1372.
31. Ashkenazy H, Erez E, Martz E, Pupko T, Ben-Tal N (2010) ConSurf 2010: Calculating evolutionary conservation in sequence and structure of proteins and nucleic acids. *Nucleic Acids Res* 38(Web Server issue):W529–W533.